

Single-PZT-Fiber Transducers for 3D Ultrasound Computed Tomography: Characterization and Modeling

Martin Angerer*, Michael Zapf*, Sylvia Gebhardt†, and Nicole V. Ruiter*

*Institute for Data Processing and Electronics, Karlsruhe Institute of Technology (KIT),
Engensteinst-Leopoldshafen, Germany, Email: Martin.Angerer@kit.edu

†Fraunhofer IKTS, Fraunhofer Institute for Ceramic Technologies and Systems, Dresden, Germany
Email: Sylvia.Gebhardt@ikts.fraunhofer.de

Abstract—In this work we present the characterization and modeling of ultrasound transducer arrays based on single-PZT-fiber transducers. The arrays were designed for a new generation of 3D ultrasound computed tomography (USCT) devices for breast cancer imaging. At the heart of the new arrays is a piezocomposite disk that features pseudo-random positioning of 18 individual transducers. Several hundred arrays were produced using semi-automated production processes and batch processing techniques. The acoustic characteristics of 54 single transducers were measured in an ultrasound testing setup. The transducers exhibit isotropic ultrasound emission, a large bandwidth (134%), and a wide opening angle (43°). This makes them well-suited for 3D USCT. A finite element model is presented for design analysis and further optimization. Initial differences between measured and modeled characteristics were reduced by adjusting piezoelectric constants, elastic properties of the passive materials and by including realistic damping in the model. As a result, the adjusted model predicts the acoustic performance over a wide range of emission angles and frequencies with good accuracy. Hence, the presented transducer arrays and the corresponding model provide a promising technology for current and future 3D USCT imaging systems.

Index Terms—ultrasound computed tomography; single-fiber transducers; finite element analysis; ultrasound testing; piezoelectric transducers

I. INTRODUCTION

A new and promising imaging method for breast cancer screening is Ultrasound Computed Tomography (USCT) [1]. In comparison with mammography and magnetic resonance imaging, ultrasound is essentially harmless, cost-effective and does not require the use of potentially harmful contrast agents [2], [3]. The general idea of USCT for breast imaging is to surround the breast by many ultrasound transducers in a fixed setup. Typically, unfocused ultrasound waves are used for the scanning. Focusing is achieved by the applied image reconstruction algorithms.

At the Karlsruhe Institute of Technology, a third-generation full 3D USCT system is currently under investigation [4]. The full 3D USCT approach enables direct reconstruction of entire breasts and is thus able to account for reflections coming from all spatial directions. Moreover, the full enclosure of the breast achieved with the 3D aperture allows for simultaneous reflection and transmission imaging [5]. These characteristics

place very challenging requirements on suitable ultrasound transducers, resulting in the necessity of a custom design.

The special requirements of the 3D USCT approach can be briefly summarized as follows: Simultaneous reflection and transmission imaging require distinct frequency ranges to achieve high resolution and a large penetration depth. Hence, the utilized ultrasound transducers should ideally exhibit a very large bandwidth (up to 180% fractional bandwidth). In order to achieve the same x-y-z resolution, the emitted acoustic field of single transducers have to be isotropic [6]. This means that the ultrasound beam shows the same spatial behavior in azimuth and elevation direction. Another important requirement is derived from the sparse imaging approach. Undersampling of the image space inevitably leads to artifacts. A suitable countermeasure to reduce these artifacts is to pseudo-randomly distribute the transducers in the aperture [4]. Furthermore, a very large opening angle (up to 60°) of the emitted sound field is required for homogeneous illumination of very large breasts [7].

A. New Array Design

In order to comply with the requirements, a new transducer array system (TAS III) design was developed, shown in Fig. 1. The design is based on a piezocomposite disk holding 18 single PZT fibers embedded in polymer (EpoTek 301-2, Epoxy Technologies). Each fiber has a thickness of 600 μm and a diameter of 460 μm . This low thickness-to-diameter ratio results from the required frequency range and opening angle. The fibers are pseudo-randomly distributed over the entire disk using a special arrange-and-fill process [8]. On the front of this piezocomposite disk, a single matching layer (microwave material TMM4, Rogers Corp.) is attached. On the back, a 4.3 mm thick PCB is connected. This PCB holds space to apply acoustic backing material (polyurethane-tungsten composite with ratio 1:2 [9]).

Each third-generation 3D USCT system accommodates 128 TAS III, resulting in a total number of 2304 transducers. To be able to produce this amount of arrays with high quality and yield, reliable manufacturing processes were needed. In order to address this challenge, we developed a semi-automated

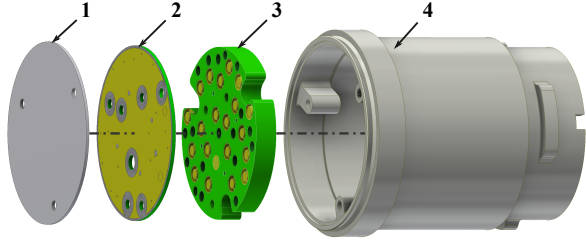


Fig. 1. New transducer array design for 3D USCT: A matching layer (1) is glued to the front of a piezocomposite disk, containing 18 spatially distributed single PZT fiber transducers (2). On the back of the piezocomposite disk, a PCB disk (3) is attached. All disks are finally integrated in a plastic housing (4).

manufacturing process [10]. Batches of 16 TAS III were processed simultaneously using automated printing and pick-and-place processes, leading to the production of more than 280 arrays. Quality control measures were developed, showing that more than 95% of the produced arrays are fully functional [11].

B. Performance Characterization

In order to assess the ultrasound characteristics of the produced TAS III, the acoustic field was measured in an ultrasound testing setup, shown in Fig. 2. In this setup, a needle hydrophone (HNC-0400, Onda Corp.) is mounted on a fully-controlled x-y-z axis. This allows for automated measurements of acoustic fields in 3D.

In the first phase of characterizing the acoustic performance, the generated acoustic field of four single transducers was measured. The hydrophone was positioned over a 120° spherical segment at a radial distance of 5 cm with a resolution of 1° . This led to 14641 measurement points and a measurement time exceeding six hours. An exemplary measurement result is shown in Fig. 3 for two frequencies within the tested frequency range (0.5 - 6 MHz). The peak in the center represents the main lobe and the concentric ring around the center illustrates the first side lobe. In general, an isotropic emission characteristic was found, with a certain variability of the emitted sound pressure within the main lobe. The higher the frequency,

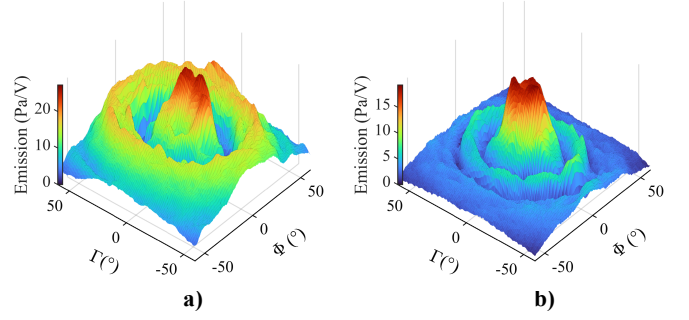


Fig. 3. Measurement of the acoustic field generated by an individual TAS III transducers at azimuth and elevation angles up to 120° at 5 cm axial distance (spherical segment). The generated field is shown at 2.5 MHz (a) and 4.3 MHz (b).

the more uniform the emission. Furthermore, the side lobe emission decreased with rising frequencies.

In the second characterization phase, a larger series of transducers was measured to be able to derive statistics. Hence, 2D measurements over 120° circular segments at 0° elevation were conducted. Figure 4 shows the average frequency- and angle-dependent sound pressure (FASP) of 54 transducers at a radial distance of 10 cm. The main lobe is present in the central angular range ($-20^\circ < \Phi < 20^\circ$), while the first side lobe is most prominent for frequencies up to 3 MHz. As indicated in Fig. 4, the FASP allows for the derivation of three main characteristics:

- The center frequency f_c , representing the frequency where the maximum sound pressure is emitted.
- The opening angle Φ_t , representing the angular width of the main lobe.
- The bandwidth bw , representing the functional frequency range.

A qualitative and quantitative comparison between the design goals and the realized TAS III is given in Tab. I. Pseudo-random positioning can be realized with the arrange-and-fill process. Isotropic emission is in principle given by the cylindrical shape of the single PZT fibers and was confirmed by the 3D characterization of the acoustic field (Fig. 3). The center frequency f_c matches the design goal very well. Larger

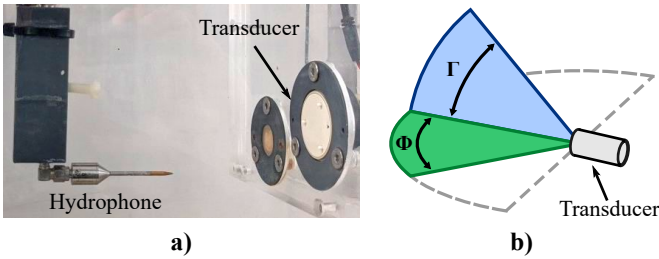


Fig. 2. Measurement setup to characterize the acoustic field of single transducers: A hydrophone is positioned at defined positions opposite of the TAS III in a water bath (a). The generated acoustic field in 3D was sampled over the azimuth plane $\Phi(^\circ)$ and elevation plane $\Gamma(^\circ)$ (b).

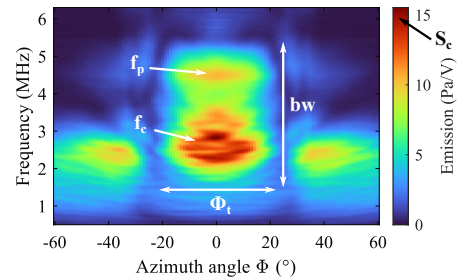


Fig. 4. Average FASP of 54 single TAS III transducers measured at 10 cm radial distance at 0° elevation angle. Five ultrasound characteristics used for statistical performance analysis and model comparison are indicated.

TABLE I
QUALITATIVE AND QUANTITATIVE ULTRASOUND CHARACTERISTICS OF
THE NEW TAS III IN COMPARISON WITH THE DESIGN GOALS.

Characteristic	Unit	Goal	TAS III
Pseudo-random positioning		Yes	Yes
Isotropic emission		Yes	Yes
Center frequency f_c	MHz	2.5	2.6 ± 0.2
Fractional bandwidth bw (-10 dB)	%	180	134.3 ± 17.7
Opening angle Φ_t (-10 dB)	°	60	42.8 ± 0.8

deviations from the ideal goal were found for the opening angle Φ_t , possibly leading to limitations in illuminating larger breasts. However, this effect is mitigated by the pseudo-random positioning and the large number of transducers in the 3D USCT system.

With a fractional bandwidth exceeding 134%, the transducers do not fully meet the design goal but still exhibit a very broadband behavior. This behavior results from two factors: First, we used a very inclusive -10 dB threshold since the electronics and signal processing of our systems provide a high dynamic range (4.6 MHz bandwidth at 54 dB gain) [12]. Second, a second resonance peak f_p (see Fig. 4) within the tested frequency range is present. This peak corresponds to the planar vibration resonance of the PZT fibers [13].

C. Modeling

Finite element analysis (FEA) was performed to accurately analyze the measured performance and potentially derive improvements for future designs. A 2D axisymmetric model was chosen since it requires low computational effort but still covers the thickness and lateral vibration modes. Full coupling of electrostatic, structural mechanic and pressure acoustic physics was applied in COMSOL Multiphysics (v5.6), enabling realistic predictions of the generated acoustic field. The piezoelectric constants were taken from the datasheet [14]. Missing constants were calculated as suggested in [15]. The elastic parameters of the utilized passive materials (filler, matching layer, backing) were taken from the datasheets or obtained by measurement [16]. A more accurate description of the model and the utilized model parameters can be found in [17].

Direct comparison between a single, representative FASP measurement and the predicted performance with the initial model is shown in Fig. 5. On first glance, the model matches the measurement well since the general emission characteristics of the main and first side lobe are largely covered. However, a significant difference was found when comparing the characteristics quantitatively. Table II lists five important characteristics (see Fig. 4), showing the relative difference between the measured average and the model predictions. S_c corresponds to the maximum emitted sound pressure at a single frequency and angle. All characteristics deviate by more than 10% from the measurement. This suggests that the mechanical properties used in the initial model do not fully match the actual conditions.

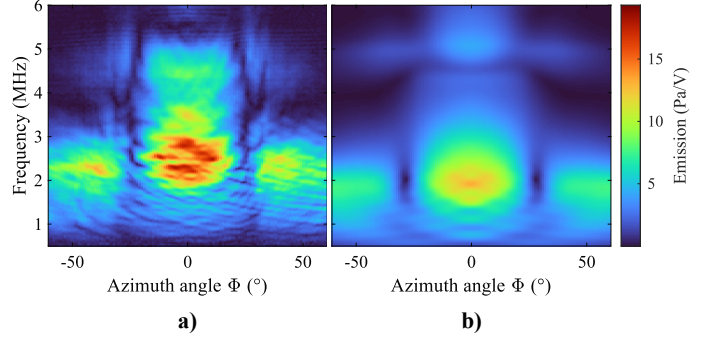


Fig. 5. Comparison of the FASP at 10 cm radial distance between a single, representative TAS III transducer measurement (a), and model predictions using parameters from literature (b).

D. Model fit

In order to improve the model predictions, the model was adjusted in two stages. In the first stage, a manual and automated parameter fit was conducted to better match the measured characteristics:

- The electromechanical coupling coefficients k_p and k_{15} as well as the piezoelectric charge constant d_{33} were reduced by 5% to lower the thickness coupling and slightly increase f_c .
- The charge constant d_{15} was increased by 6% to pronounce the planar resonance f_p .
- The density of the piezoelectric material was reduced to match conducted measurements. This leads to an increase in f_c .
- The Young's modulus of the composite material was increased by 20% to realize a higher stiffness. This leads to a decrease in Φ_t .
- The elastic compliances s_{33}^E and s_{11}^E were reduced until a match of 5% in f_c and f_p was achieved using a brute-force approach.

Each change of piezoelectric properties was followed by a full conversion of the piezoelectric parameter matrix (in strain-charge form) in order to retain a consistent set of constants.

In the second stage of improving the model predictions, realistic damping properties of the utilized passive materials were considered. These parameters were obtained by deriving the frequency-dependent sound attenuation using an ultrasound transmission setup [16]. A previously developed method to convert sound attenuation into an equivalent structural loss factor was applied [18]. The resulting frequency-dependent loss factors were finally integrated in the FEA.

The predicted FASP of the improved model in comparison with the single measurement is shown in Fig. 6. Now, the model agrees well with the measurement, providing good predictions also for frequencies above 3 MHz. The quantitative comparison in Tab. II shows that all but one characteristic fits better with the measured average. The rise in bw is caused by the larger attenuation and results from an increased sound pressure at frequencies below f_c . This must be considered

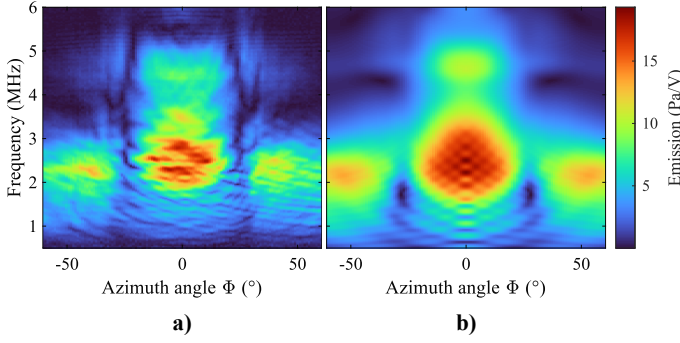


Fig. 6. Comparison of the measured FASP (a) and the model after improving the model predictions by adjusting parameters and considering realistic damping properties (b).

TABLE II

MEASURED (AVERAGE) ULTRASOUND CHARACTERISTICS OF THE TAS III TRANSDUCERS AND THE RELATIVE DIFFERENCE IN PERCENT OF THE INITIAL AND IMPROVED MODEL.

	f_c	f_p	bw	Φ_t	S_c
Measurement	2.6 MHz	4.5 MHz	134.3%	42.8°	18.6 Pa/V
Initial model	-23%	+13%	+12%	+23%	-29%
Improved model	-5%	+3%	+22%	+14%	-4%

when analyzing future designs, especially with respect to transmission imaging. Still, the improved model is well-suited for investigating measured effects and identifying further design improvements.

II. CONCLUSION

In the first part of this paper, we present new transducer arrays for a third-generation 3D USCT device for breast cancer screening. The developed technology enables the realization of sparse piezocomposite arrays with random positioning of PZT fibers. The developed manufacturing processes enable fast and reliable production of larger series. Ultrasound characterization showed isotropic emission characteristics, a very large bandwidth (134%), and large opening angles (43°). Most of the requirements were fulfilled, though a even larger bandwidth and opening angle would be desirable. Still, the realized arrays are well-suited for 3D USCT imaging.

In the second part of the paper, a finite element model of the realized transducers is presented. The model was developed for detailed analyses of the design and identification of further improvements. Larger initial differences between measured and modeled characteristics were reduced by adjusting several parameters within a limited range and by including realistic damping properties in the model. The adjusted model predicts the acoustic performance of individual transducers over a wide range of emission angles and frequencies with good accuracy. Hence, the model complements the developed technology and reduces the necessity for future prototyping.

REFERENCES

- [1] N. Duric, P. Littrup, C. Li, O. Roy, S. Schmidt, R. Janer, X. Cheng, J. Goll, O. Rama, L. Bey-Knight, and W. Greenway, "Breast ultrasound tomography: Bridging the gap to clinical practice," *Progress in Biomedical Optics and Imaging - Proceedings of SPIE*, vol. 8320, p. 23, 2012.
- [2] L. Lin, P. Hu, J. Shi, C. M. Appleton, K. Maslov, L. Li, R. Zhang, and L. V. Wang, "Single-breath-hold photoacoustic computed tomography of the breast," *Nature Communications*, vol. 9, no. 1, p. 2352, 2018.
- [3] K. J. Opieliński, P. Pruchnicki, T. Gudra, P. Podgórski, J. Kurcz, T. Krasnicki, M. Sasiadek, and J. Majewski, "Imaging results of multi-modal ultrasound computerized tomography system designed for breast diagnosis," *Computerized Medical Imaging and Graphics*, vol. 46, pp. 83–94, 2015.
- [4] H. Gemmeke, L. Berger, T. Hopp, M. Zapf, W. Tan, R. Blanco, R. Leys, I. Peric, and N. V. Ruiter, "The new generation of the KIT 3D USCT," in *International Workshop on Medical Ultrasound Tomography*, vol. 1, pp. 271–281, KIT Scientific Publishing, 2018.
- [5] N. V. Ruiter, M. Zapf, R. Dapp, T. Hopp, W. A. Kaiser, and H. Gemmeke, "First results of a clinical study with 3D ultrasound computer tomography," in *2013 IEEE International Ultrasonics Symposium (IUS)*, pp. 651–654.
- [6] N. Ruiter, G. Göbel, L. Berger, M. Zapf, and H. Gemmeke, "Realization of an optimized 3D USCT," in *2011 Proceedings of SPIE*, vol. 7968.
- [7] M. Zapf, P. Pfister, C. I. Liberman, K. W. A. Van Dongen, B. Leyrer, H. Gemmeke, and N. V. Ruiter, "Dice-and-fill single element octagon transducers for next generation 3D USCT," in *International Workshop on Medical Ultrasound Tomography*, pp. 159–177, KIT Scientific Publishing, Karlsruhe, 2017.
- [8] S. E. Gebhardt, K. Hohlfeld, P. Günther, and H. Neubert, "Manufacturing technologies for ultrasonic transducers in a broad frequency range," in *Proceedings of the International Workshop on Medical Ultrasound Tomography*, (Speyer), pp. 147–158, 2017.
- [9] M. Zapf, K. Hohlfeld, N. V. Ruiter, P. Pfister, K. W. A. van Dongen, H. Gemmeke, A. Michaelis, and S. E. Gebhardt, "Development of single-fiber piezocomposite transducers for 3D ultrasound computer tomography," *Adv. Eng. Mater.*, vol. 20, p. 1800423, 2018.
- [10] M. Angerer, M. Zapf, B. Leyrer, and N. V. Ruiter, "Semi-automated packaging of transducer arrays for 3D ultrasound computer tomography," in *Proceedings of 2020 IEEE Sensors*, IEEE.
- [11] M. Angerer, M. Zapf, M. Koch, and N. V. Ruiter, "Quality control of ultrasound transducers using distribution-free overlapping coefficients," in *Proceedings of 2021 IEEE Sensors*, IEEE.
- [12] Z. Lu, R. Blanco, K. Schlote-Holubek, M. Zapf, H. Gemmeke, I. Perić, and N. V. Ruiter, "Novel front-end design with high-voltage transceiver ASICs for ultrasound computed tomography," in *2021 IEEE International Ultrasonics Symposium (IUS)*.
- [13] M. Angerer, M. Zapf, S. Gebhardt, H. Neubert, and N. V. Ruiter, "Enhanced KLM model for single-fibre piezocomposite transducers," in *Proceedings of 2020 IEEE Ultrasonics*, IEEE.
- [14] CeramTec GmbH, Plochingen, Germany, *Material Datasheet SONOX P505*. 2019.
- [15] G. Chevallier, S. Ghorbel, and A. Benjeddou, "A benchmark for free vibration and effective coupling of thick piezoelectric smart structures," *Smart Materials and Structures*, vol. 17, p. 065007, 2008.
- [16] J. Koppenhöfer, *Measurement Environment for Acoustic Material Properties for Ultrasound Computed Tomography*. Master Thesis, Karlsruhe Institute of Technology, 2020.
- [17] M. Angerer, *Transducer Arrays for 3D Ultrasound Computed Tomography*. Phd thesis, Karlsruhe Institute of Technology, 2022, Manuscript submitted for publication.
- [18] M. Angerer, M. Zapf, J. Koppenhöfer, and N. V. Ruiter, "Method to extract frequency dependent material attenuation for improved transducer models," in *Proceedings of 2021 IEEE Ultrasonics*.